Numerical Simulation of Hypervelocity Projectiles in Detonable Gases

S. Yungster,* S. Eberhardt,† and A. P. Bruckner‡
University of Washington, Seattle, Washington 98195

A numerical scheme for calculating hypersonic flows involving shock-induced combustion is discussed. The analysis is limited to inviscid flow and includes chemical nonequilibrium and real-gas effects. Two types of flows are considered. First, the hypersonic, exothermic blunt-body flow problem is examined for mixtures of H_2/O_2 and H_2/air, and the numerical results are compared with experimental results. Second, a hypervelocity mass launcher concept known as the "ram accelerator" is investigated in the velocity range of 5–7 km/s. Temperature contours and the distribution of various physical quantities along the ram accelerator projectile surface and tube wall are presented for a 14-deg nose projectile and for a gas mixture of $2H_2 + O_2 + 5He$.

Introduction

THE possibility of using shock-induced combustion in hypersonic airbreathing engines and hypersonic mass launchers has been investigated during the last few years. Such an approach has been considered as an alternative to the supersonic combustion ramjet for propelling space transportation vehicles such as the NASP (National Aerospace Plane) in a configuration known as the Oblique Detonation Wave Engine (ODWE).[1,2]

Also, at the University of Washington, experimental and theoretical research is being carried out on the acceleration of projectiles to high velocities using a ramjet-in-tube concept called the "ram accelerator."[3-6] The projectile, which resembles the centerbody of a conventional ramjet, is accelerated by combustion through a tube filled with a reactive mixture (see Fig. 1). Several modes of ram accelerator operation, which span the velocity range of 0.7–12 km/s, have been proposed, with some of them (like the one shown in Fig. 1) using oblique detonation waves or a shock-deflagration system as the energy release mechanism.

Both the ODWE and the ram accelerator are designed to ignite a premixed fuel/oxidizer mixture by means of a series of shock waves that increase its temperature until the ignition temperature is reached at some desired location. At this point, rapid chemical reactions release energy into the flowing stream. The energy addition, however, will not necessarily establish a detonation wave, as it is also possible that the reaction will produce either a coupled or decoupled shock-deflagration system.

Such shock-induced combustion phenomena, ranging from decoupled shock-deflagration systems to overdriven detonation waves, were experimentally investigated in the mid-1960s[7,8] and early 1970s, most notably by Behrens et al.[9] and Lehr.[10] Their experiments consisted of firing spheres and other projectiles through explosive mixtures of H_2/O_2 and H_2/air. These experiments, covering a wide range of shock-induced combustion modes, can be used as test cases for numerical schemes being used to calculate hypersonic chemically reacting flows.

Presented as Paper 89-0673 at the AIAA 27th Aerospace Sciences Meeting, Reno, NV, Jan. 9-12, 1989; received May 11, 1989; revision received March 14, 1990.

*Research Assistant, Department of Aeronautics and Astronautics; currently, Research Associate, Institute for Computational Mechanics in Propulsion, Cleveland, OH. Member AIAA.

†Assistant Professor, Department of Aeronautics and Astronautics. Member AIAA.

‡Research Professor, Department of Aeronautics and Astronautics. Associate Fellow AIAA.

In the present study, a new numerical scheme developed for calculating hypersonic chemically reacting flows is described. The new numerical formulation represents a departure from previous computational fluid dynamics models of the ram accelerator.[11,12] The earlier models were based on a global Arrhenius rate equation, with the Arrhenius constants determined from experimental ignition delay studies. The current model is more accurate in that it accounts for the reaction kinetics of a 7 species 8 reaction combustion model. Nonetheless, the earlier results were encouraging in that they predicted hypervelocity operation was possible.

The new scheme, based on an algorithm developed by Yee and Shinn,[13] was applied to spheres moving through mixtures of H_2/O_2 and H_2/air at speeds above and below the corresponding Chapman-Jouguet detonation speed. The results were then compared with the experiments just mentioned. The code was also used to investigate the flow and combustion processes in the ram accelerator, in the velocity range of 5–7 km/s.

The first section of this paper presents an overview of the phenomena associated with hypersonic exothermic blunt-body flow. The following sections describe the governing equations, combustion model, and the numerical scheme used. Finally, results are presented for hypersonic blunt-body flows and for a complete ram accelerator configuration.

Regimes of Exothermic Blunt-Body Flow

Figure 2 shows the structure of the shock layer in the vicinity of the stagnation point of a blunt body moving through a detonable gas mixture. At flight speeds U_1, sufficiently low such that the temperature behind the bow shock is less than the ignition temperature, no combustion will occur. At higher flight speeds, but still below the detonation speed D of the gas mixture, the shock and combustion front are separated by an induction zone of thickness Δ_i. This situation is shown in Fig. 3, obtained from the work of Lehr,[10] for a stoichiometric

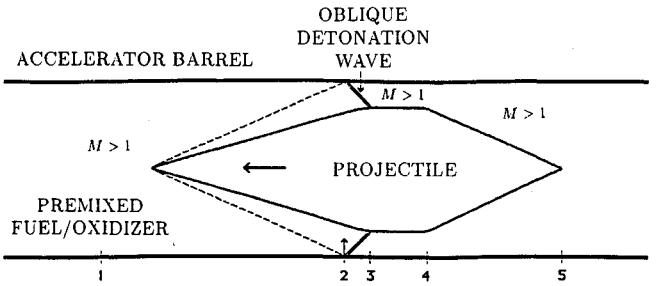

Fig. 1 Schematic of oblique detonation ram accelerator drive mode.

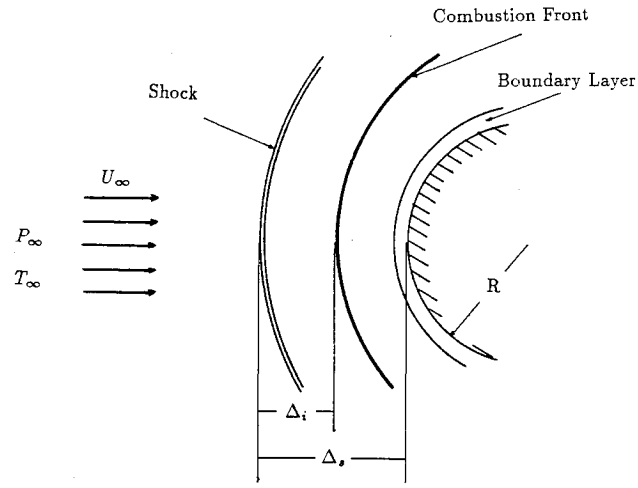

Fig. 2 Characteristic lengths in exothermic blunt-body flow.

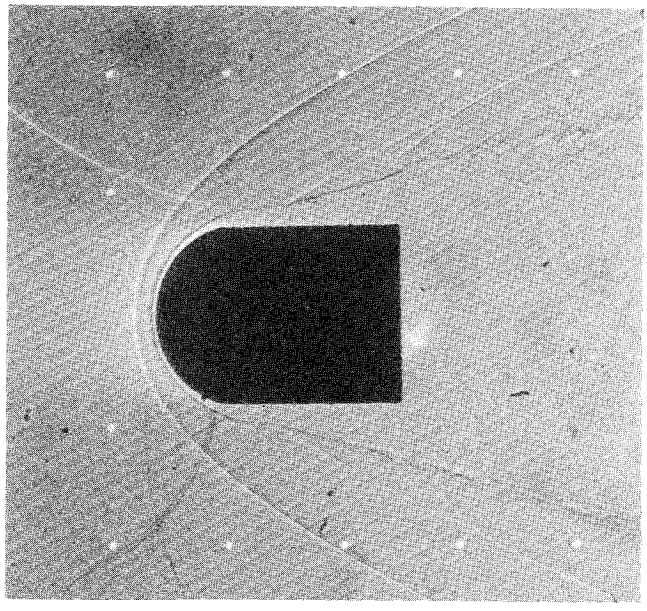

Fig. 3 Shock wave and combustion front at subdetonative speed ($U_1 < D$, $M = 3.55$) in a stoichiometric H_2/O_2 mixture (Ref. 10).

mixture of H_2/O_2. A similar result is obtained for a stoichiometric mixture of H_2/air. When the flight speed is very close to the Chapman-Jouguet value, the reaction shows pulsations of constant frequency for the H_2/air mixture, and a normal Chapman-Jouguet detonation propagating in front of the model for the H_2/O_2 mixture. If the model is flying at speeds above the detonation speed, the induction zone and combustion front merge to form a combination of overdriven and oblique detonation waves for the H_2/O_2 mixture (Fig. 4) and a coupled shock-deflagration system for the H_2/air mixture (Fig. 5).[10]

Our objective is to numerically reproduce the experimental results just described for subdetonative speeds ($U_1 < D$) and superdetonative speeds ($U_1 > D$). These numerical simulations will provide the code validation needed for subsequent applications to the ram accelerator configuration.

The cases involving flight speeds very close to the Chapman-Jouguet speed represent a very difficult subject, since they involve unsteady phenomena, and remain a topic for future research.

Governing Equations

Our analysis will be limited at the present time to inviscid flow. For the case of chemically reacting flows, the Euler

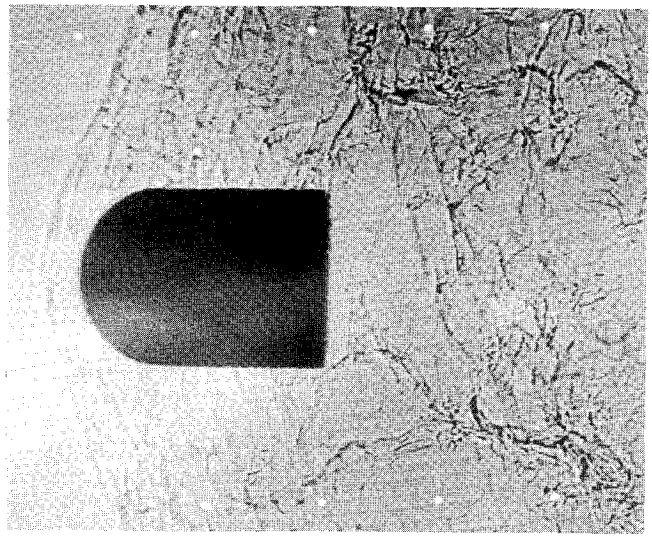

Fig. 4 Overdriven detonation and oblique Chapman-Jouguet detonation for superdetonative speed ($U_1 > D$, $M = 5.08$) in a stoichiometric H_2/O_2 mixture (Ref. 10).

equations, with the global continuity equation replaced by all the species continuity equations, are used. They can be expressed in the following conservation form for a gas containing n species and in general curvilinear coordinates (ξ,η)

$$\frac{\partial q}{\partial t} + \frac{\partial F}{\partial \xi} + \frac{\partial G}{\partial \eta} + jH = W \tag{1}$$

where

$$q = J^{-1}\begin{bmatrix} \rho_1 \\ \rho_2 \\ \vdots \\ \rho_n \\ \rho u \\ \rho v \\ e \end{bmatrix}, \qquad F = J^{-1}\begin{bmatrix} \rho_1 U \\ \rho_2 U \\ \vdots \\ \rho_n U \\ \rho u U + \xi_x p \\ \rho v U + \xi_y p \\ U(e+p) \end{bmatrix}$$

$$G = J^{-1}\begin{bmatrix} \rho_1 V \\ \rho_2 V \\ \vdots \\ \rho_n V \\ \rho u V + \eta_x p \\ \rho v V + \eta_y p \\ V(e+p) \end{bmatrix}, \qquad H = (J^{-1}/y)\begin{bmatrix} \rho_1 v \\ \rho_2 v \\ \vdots \\ \rho_n v \\ \rho u v \\ \rho v^2 \\ v(e+p) \end{bmatrix}$$

$$W = J^{-1}\begin{bmatrix} w_1 \\ w_2 \\ \vdots \\ w_n \\ 0 \\ 0 \\ 0 \end{bmatrix} \tag{2}$$

The equations describe two dimensional flow if $j = 0$ and axisymmetric flow if $j = 1$. The variables are the velocity com-

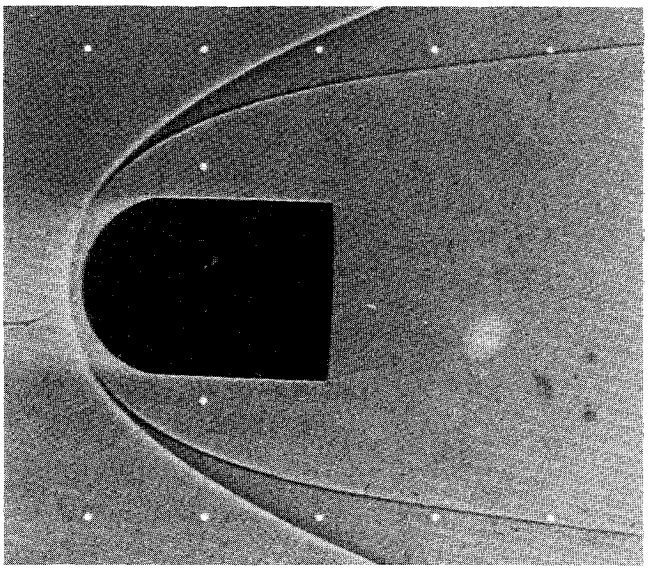

Fig. 5 Shock-deflagration system for superdetonative speed ($U_1 > D$, $M = 6.46$) in a stoichiometric H_2/air mixture (Ref. 10).

ponents u and V, the pressure p, the energy-per-unit volume e, and the density of the ith species ρ_i, with $\rho = \Sigma_{i=1}^{n} \rho_i$. The terms w_i represent the production of species from chemical reactions and are calculated by standard methods.[14] The variable y is the cylindrical radius. Finally, the grid Jacobian J and the contravariant velocities U and V are defined as follows

$$J^{-1} = x_\xi y_\eta - x_\eta y_\xi$$

$$U = \xi_x u + \xi_y v, \qquad V = \eta_x u + \eta_y v$$

$$\xi_x = J y_\eta, \qquad \xi_y = -J x_\eta$$

$$\eta_x = -J y_\xi, \qquad \eta_y = J x_\xi \tag{3}$$

The terms x_ξ, x_η, etc., are the grid metric terms $(\partial x/\partial \xi)$, $(\partial x/\partial \eta)$, etc. The equation of state used is that for a mixture of thermally perfect gases

$$p = \sum_{i=1}^{n} \frac{\rho_i}{M_i} RT \tag{4}$$

where M_i is the molecular weight of the ith species, and R is the universal gas constant. The temperature T is determined from the definition of the total energy:

$$\sum_{i=1}^{n} c_i \int^{T} c_{v_i}\, dT = \frac{e}{\rho} - \frac{1}{2}(u^2 + v^2) - \sum_{i=1}^{n} c_i h_i^0 \tag{5}$$

where $c_i = (\rho_i/\rho)$, c_{v_i} is the specific heat at constant volume of the ith species, and h_i^0 is the heat of formation for species i. Expressions for the specific heats as a function of temperature are obtained from the JANNAF tables[15] and use the following polynomial fit[16]

$$(c_{p_i}/R) = A_1 + A_2 T + A_3 T^2 + A_4 T^3 + A_5 T^4$$

where c_{p_i} is the specific heat at constant pressure of the ith species, and $A_1, \ldots, A_5$ are constants. It should be mentioned that recent work by Wada et al.[17] has shown that the assumption of constant specific heat in calculating chemically reacting flows can lead to large errors because temperatures (on which the reaction rates strongly depend) tend to be overestimated.

Combustion Model

The combustion model used for the present study is the one proposed by Moretti[18] that consists of six reacting species H, O, H_2O, OH, O_2, H_2, and an inert species such as argon or nitrogen. Eight reactions are assumed to be significant:

$$H + O_2 \rightleftharpoons OH + O$$

$$O + H_2 \rightleftharpoons OH + H$$

$$H_2 + OH \rightleftharpoons H + H_2O$$

$$2OH \rightleftharpoons O + H_2O$$

$$H_2 + X \rightleftharpoons 2H + X$$

$$H_2O + X \rightleftharpoons OH + H + X$$

$$OH + X \rightleftharpoons O + H + X$$

$$O_2 + X \rightleftharpoons 2O + X$$

The forward and backward reaction rates for the ith reaction, K_{fi} and K_{bi}, are given by expressions of the form

$$K_i = A_i T^{b_i} e^{-C_i/T} \tag{6}$$

The reaction coefficients A_i, b_i, and C_i were taken from Evans and Schexnayder,[19] who also analyzed hydrogen/air supersonic flames using the preceding system of seven species and eight reactions. They compared the results to those obtained with a system consisting of 12 species and 25 reactions. The main difference between the 8-reaction and the 25-reaction model was the addition of HO_2, NO, and NO_2. Reactions involving HO_2 (hydroperoxide) are important for low-temperature ignition studies. The main conclusions of their study are the following:

1) Although the 25-reaction model is superior to the 8-reaction model for predicting ignition (due to the presence of more reaction paths for the creation and depletion of free radicals such as H, O, and OH), once ignition occurs, the 8-reaction model results are as good as those from the 25-reaction model.

2) In a system where external means for ignition are provided or where spontaneous ignition is known to be fast, the 8-reaction system is a good approximation.

More complicated models for hydrogen combustion have also been proposed.[20,21] These include more reaction paths than the 25-reaction model and also include reactions involving H_2O_2 (hydrogen peroxide). For the ram accelerator studies, the inclusion of HO_2 and H_2O_2 could be important at the lower Mach number flight regime, where low-temperature ignition occurs. At higher Mach numbers, such species are probably unimportant.

Numerical Method

The equation set describing chemically reacting flows is difficult to solve because it is mathematically stiff. Stiffness can be defined as the ratio of the largest to the smallest time scale. In reacting flows, the time scales associated with the chemisty tend to be much smaller than the time scale of fluid motion, sometimes by orders of magnitude. For the equation set being discussed here, the degree of stiffness is determined by the ratio of the characteristic convection time τ_{conv} to the characteristic reaction time τ_{ch}, a parameter known as the Damköhler number

$$Da = \frac{\tau_{\text{conv}}}{\tau_{ch}} \tag{7}$$

In general, there will be one Damköhler number associated with each chemical reaction.

There are currently two approaches to solving stiff systems of equations. One approach is to uncouple the fluid dynamics equations from the rate equations. Each time step consists of a fluid dynamics step with frozen chemistry followed by a

chemical reaction step (or several small steps) without flow interaction.[11,22] The second approach solves the fully coupled equation set simultaneously. This approach requires an implicit treatment of the chemical source terms that, as shown by Bussing and Murman,[23] essentially rescales the equations in time so that all events occur on a similar pseudotime scale. In the past few years, several algorithms have been developed for calculating nonequilibrium flows based on this approach.[13,17,23,24]

In this paper, the fully coupled equation set is solved using a numerical scheme based on a total variation diminishing (TVD) algorithm developed by Yee and Shinn,[13] sometimes referred to as the "point implicit TVD MacCormack" scheme. In generalized coordinates and for a grid spacing $\Delta\xi = \Delta\eta = 1$, it is given by

Predictor:

$$\boldsymbol{D}^n_{j,k}\Delta\boldsymbol{q}^{(1)}_{j,k} = -\Delta t(\boldsymbol{F}^n_{j,k} - \boldsymbol{F}^n_{j-1,k} + \boldsymbol{G}^n_{j,k+1} - \boldsymbol{G}^n_{j,k}) + \Delta t\boldsymbol{W}^n_{j,k} \quad (8)$$

$$\boldsymbol{q}^{(1)}_{j,k} = \Delta\boldsymbol{q}^{(1)}_{j,k} + \boldsymbol{q}^n_{j,k} \quad (9)$$

Corrector:

$$\boldsymbol{D}^1_{j,k}\Delta\boldsymbol{q}^{(2)}_{j,k} = \tfrac{1}{2}\left[-\Delta\boldsymbol{q}^{(1)}_{j,k} - \Delta t(\boldsymbol{F}^{(1)}_{j+1,k} - \boldsymbol{F}^{(1)}_{j,k} + \boldsymbol{G}^{(1)}_{j,k} - \boldsymbol{G}^{(1)}_{j,k-1})\right] + (\Delta t/2)\boldsymbol{W}^{(1)}_{j,k} \quad (10)$$

$$\boldsymbol{q}^{(2)}_{j,k} = \Delta\boldsymbol{q}^{(2)}_{j,k} + \boldsymbol{q}^{(1)}_{j,k} \quad (11)$$

$$\boldsymbol{q}^{n+1}_{j,k} = \boldsymbol{q}^{(2)}_{j,k} + (\boldsymbol{R}^n_{j+\frac{1}{2}}\boldsymbol{\Phi}^n_{j+\frac{1}{2}} - \boldsymbol{R}^n_{j-\frac{1}{2}}\boldsymbol{\Phi}^n_{j-\frac{1}{2}}) + (\boldsymbol{R}^n_{k+\frac{1}{2}}\boldsymbol{\Phi}^n_{k+\frac{1}{2}} - \boldsymbol{R}^n_{k-\frac{1}{2}}\boldsymbol{\Phi}^n_{k-\frac{1}{2}}) \quad (12)$$

where $\boldsymbol{R}_{j\pm\frac{1}{2}}$ denotes the matrix of eigenvectors of the flux Jacobian matrix $\boldsymbol{A} = (\partial\boldsymbol{F}/\partial\boldsymbol{q})$ evaluted at some symmetric average of $\boldsymbol{q}_{j,k}$ and $\boldsymbol{q}_{j+1,k}$, denoted as $\boldsymbol{q}_{j\pm\frac{1}{2}}$, and $\boldsymbol{R}_{k\pm\frac{1}{2}}$ denotes the matrix of eigenvectors of the flux Jacobian matrix $\boldsymbol{B} = (\partial\boldsymbol{G}/\partial\boldsymbol{q})$ evaluated at $\boldsymbol{q}_{k\pm\frac{1}{2}}$. The "scaling matrix" $\boldsymbol{D}$ is given by

$$\boldsymbol{D}^n = \left(\boldsymbol{I} - \Delta t\theta\frac{\partial\boldsymbol{W}}{\partial\boldsymbol{q}}\right), \qquad \boldsymbol{D}^1 = \left(\boldsymbol{I} - \frac{\Delta t}{2}\theta\frac{\partial\boldsymbol{W}}{\partial\boldsymbol{q}}\right) \quad (13)$$

where Δt is the time step, and θ is a parameter in the range $0 \le \theta \le 1$. All of our calculations were done with $\theta = 1$ for maximum numerical stability. The elements $\phi^l_{j+\frac{1}{2}}$ of the dissipation vector $\boldsymbol{\Phi}_{j+\frac{1}{2}}$ are

$$\phi^l_{j+\frac{1}{2}} = \tfrac{1}{2}\left[\Psi(\nu^l_{j+\frac{1}{2}}) - (\nu^l_{j+\frac{1}{2}})^2\right]\left[\alpha^l_{j+\frac{1}{2}} - \hat{Q}^l_{j+\frac{1}{2}}\right] \quad (14)$$

$$\nu^l_{j+\frac{1}{2}} = \Delta t a^l_{j+\frac{1}{2}} \quad (15)$$

$$\boldsymbol{\alpha}_{j+\frac{1}{2}} = \boldsymbol{R}^{-1}_{j+\frac{1}{2}}(\boldsymbol{q}_{j+1,k} - \boldsymbol{q}_{j,k}) \quad (16)$$

where $a^l_{j+\frac{1}{2}}$ denotes the eigenvalues of $\boldsymbol{A}$ evaluated at $\boldsymbol{q}_{j+\frac{1}{2}}$, and $\alpha^l_{j+\frac{1}{2}}$ denotes the elements of the vector $\boldsymbol{\alpha}_{j+\frac{1}{2}}$. The function Ψ is

$$\Psi(z) = \begin{cases} |z| & |z| \ge \epsilon \\ \dfrac{(z^2+\epsilon^2)}{2\epsilon} & |z| < \epsilon \end{cases} \quad \text{for } 0.05 \le \epsilon \le 0.2 \quad (17)$$

The "limiter" function $\hat{Q}_{j+\frac{1}{2}}$ used in this study is given by

$$\hat{Q}^l_{j+\frac{1}{2}} = \text{minmod}(\alpha^l_{j-\frac{1}{2}}, \alpha^l_{j+\frac{1}{2}}, \alpha^l_{j+3/2}) \quad (18)$$

Alternative forms of the "limiter" function are given in Ref. 13. The eigenvalues and eigenvectors of the fully coupled chemically reacting equations were obtained by Eberhardt and Brown[25] in Cartesian coordinates. They have been extended to generalized coordinates and used for calculating the vectors $\boldsymbol{R}\boldsymbol{\Phi}$ apearing in Eq. (12). The resulting expressions for $\boldsymbol{R}\boldsymbol{\Phi}$ are given in the Appendix. This scheme is second-order accurate in space and is suitable for steady-state calculations.

Before moving on to describe the results obtained with this scheme it should be mentioned that when coupling chemical energy release to fluid dynamics, problems can arise when the chemical reactions are very fast (i.e., very large Damköhler numbers). For very fast chemistry, most of the heat release takes place in a very short distance behind the shock wave, and if the grid resolution is not high enough to capture this process, errors in the computed quantities, including temperature, can occur. Because of the strong dependence of the reaction rates on temperature, this situation can cause the release of energy much sooner than it should be released. The result can be runaway chemical reactions and nonphysical flame or detonation velocities. One way to prevent this problem is to limit the Damköhler number to a value such that the heat release is distributed among at least two or three cells. This approach was taken in the present study; alternative approaches to this problem are discussed by Oran and Boris.[26]

Results

A. Exothermic Blunt-Body Flows

Calculations were carried out for a sphere having a diameter of 15 mm, moving through stoichiometric mixtures (equivalence ratio $\phi = 1$) of H_2/O_2 and H_2/air, at pressures of 186 and 320 Torr, respectively, for each mixture. These conditions reproduce those of the experiments shown in Figs. 3-5.[10] The measured detonation speed of each mixture is[10]

H_2/O_2 $\quad D = 2550$ m/s

H_2/air $\quad D = 2055$ m/s

The results of these calculations are presented in Figs. 6-11, which are discussed below. All of the calculations presented here were carried out on a 42×44 orthogonal grid. The same calculations were also conducted on a 32×32 grid. The effect of a coarser grid was evident mainly in the increased thickness of the captured shocks. The overall computed shock-combustion structure remained independent of the grid size.

1. *Subdetonative Speeds*

Figure 6 shows the temperature contours obtained using the numerical scheme for the H_2/O_2 mixture at a projectile speed $U_1 = 1892$ m/s ($M = 3.55$). This condition corresponds to Fig. 3. The shock wave, induction zone, and combustion front can be clearly identified. The shock location as taken from Fig. 3 is also shown for comparison. The predicted shock location is slightly farther out from the body than the experimental location, probably due to a slightly thicker computed combustion zone.

The distribution of physical quantities on the stagnation line is shown in Fig. 7. The temperature plot shows the jump across the shock followed by a constant value during the induction time and a subsequent increase during the combustion phase. The pressure distribution is nearly unaffected by the heat release, and as a result, the change in density must be opposite to that of temperature in the combustion zone.

Calculations were also carried out for the H_2/air mixture at a speed of $U_1 = 1685$ m/s. Very good agreement between the computed and the experimentally observed shock and combustion front location was obtained.

2. *Superdetonative Speeds*

When the body is flying at superdetonative speeds, i.e., speeds above the detonation speed of the mixture, a coupled shock and combustion front is formed whose structure depends on the mixture. Figure 8 shows the results for the H_2/O_2 mixture and a projectile speed $U_1 = 2705$ m/s ($M = 5.08$) that corresponds to Fig. 4. A combination of overdriven and

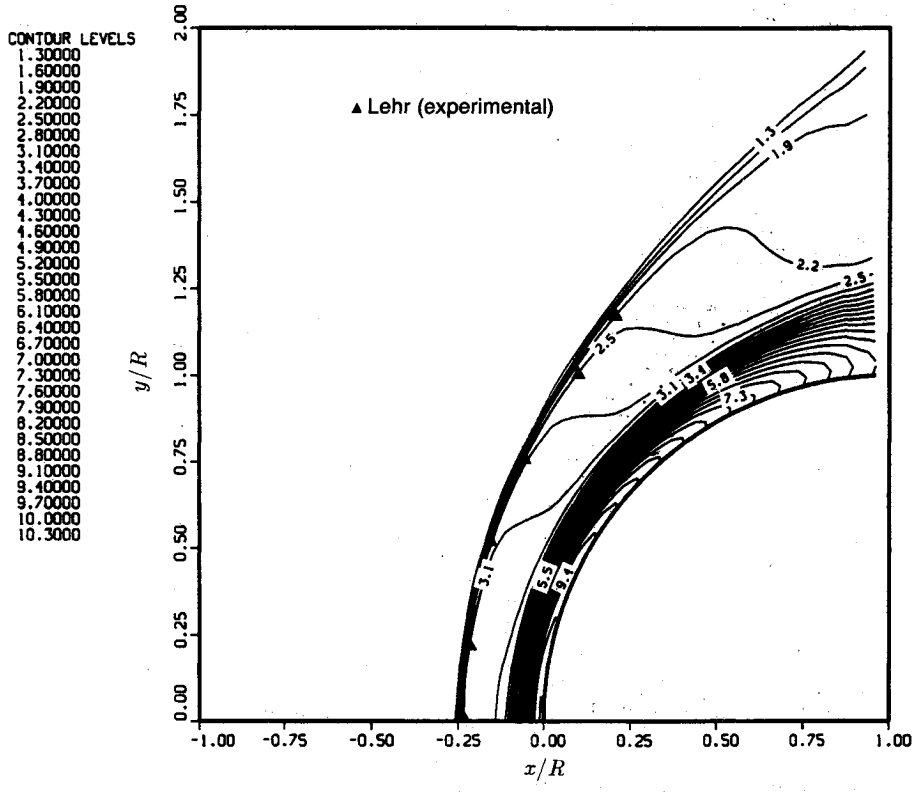

Fig. 6 Temperature contours (T/T_∞) for stoichiometric H_2/O_2, $M = 3.55$ flow past a sphere. Experimental shock location obtained from Fig. 3 (Ref. 10).

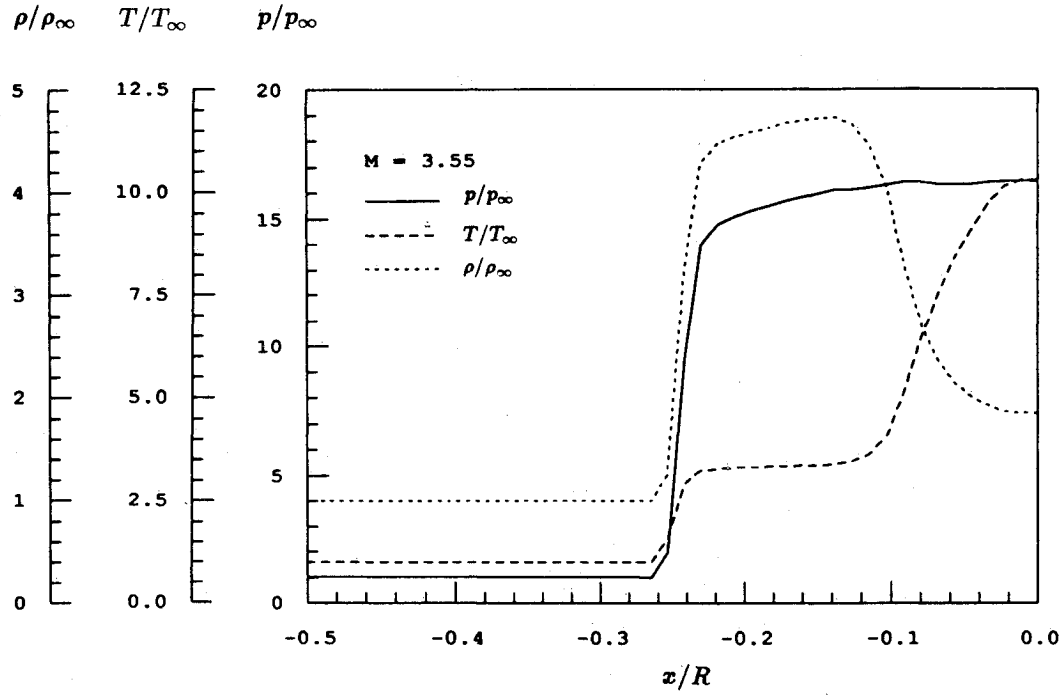

Fig. 7 Distribution of physical quantities along the stagnation streamline for $M = 3.55$ flow past a sphere in a mixture of H_2/O_2.

oblique detonation waves is obtained. Although the detailed structure of the detonation cannot be resolved, the overall effects, such as the location of the overdriven portion of the detonation wave and the angle of the oblique portion, are in close agreement with the experiment.

The temperature plot shown in Fig. 9 shows that the heat release occurs immediately behind the shock. It is interesting to observe that the pressure plot exhibits a von Neumann spike not observed in nonreacting flows.

Figure 10 shows the results for the H_2/air mixture. The projectile speed is $U_1 = 2605$ m/s ($M = 6.46$) corresponding to Fig. 5. In this case, the energy release is not high enough to initiate a detonation, and this fact is also reflected in the numerical calculation. Because of the smaller ratio of chemical energy to kinetic energy, the influence of heat release on the flow is not as strong as for the previous case (see Fig. 11), and for the same reason, the von Neumann spike is not observed in this case.

The $M = 6.46$ case of Fig. 5 was studied also by Lee and Deiwert[27] using the F3d/Chem code. The chemistry model and the rate coefficients used by Lee and Deiwert are the same as in the present study. The results of their calculations are in close agreement with those obtained with the present method (shown in Fig. 11).

The benchmark computations presented here are in very good agreement with the experimental results, with respect to the shock-wave and combustion front locations. This is a sensitive test since the shock location and shape are strongly dependent on the amount of heat release in the reaction zone. In what follows we present results obtained for a ram accelerator configuration.

B. Ram Accelerator Configuration

The gasdynamic principles of the ram accelerator (Fig. 1) are similar to those of a conventional airbreathing ramjet[3-6]; however, the device is operated in a different manner. The projec-

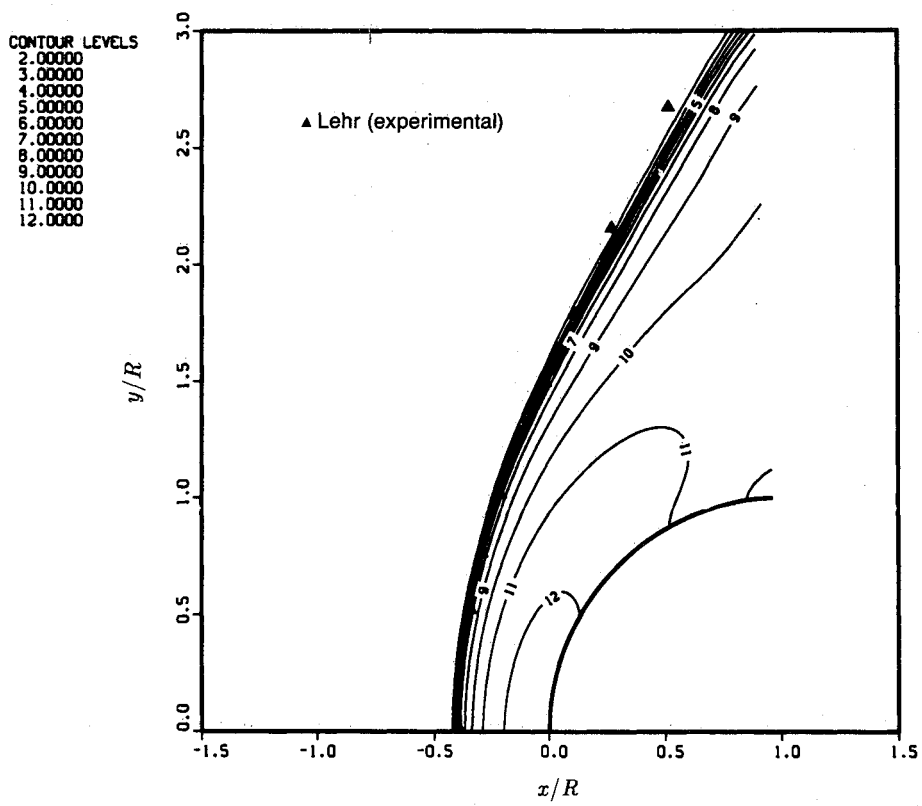

Fig. 8 Temperature contours (T/T_∞) for stoichiometric H_2/O_2, $M = 5.08$ flow past a sphere. Experimental shock location obtained from Fig. 4 (Ref. 10).

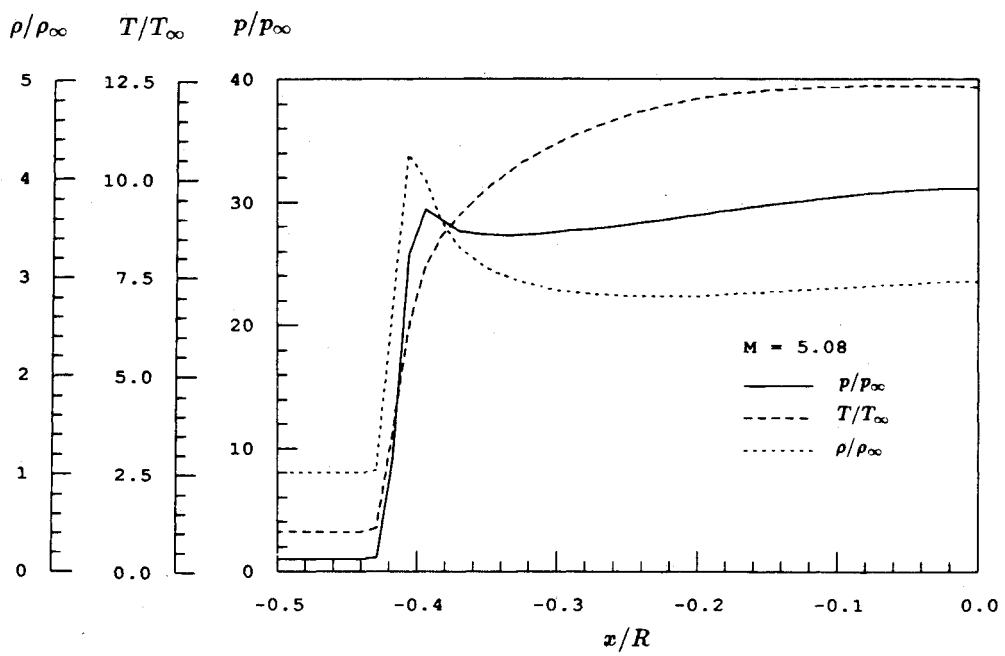

Fig. 9 Distribution of physical quantities along the stagnation streamline for $M = 5.08$ flow past a sphere in a mixture of H_2/O_2.

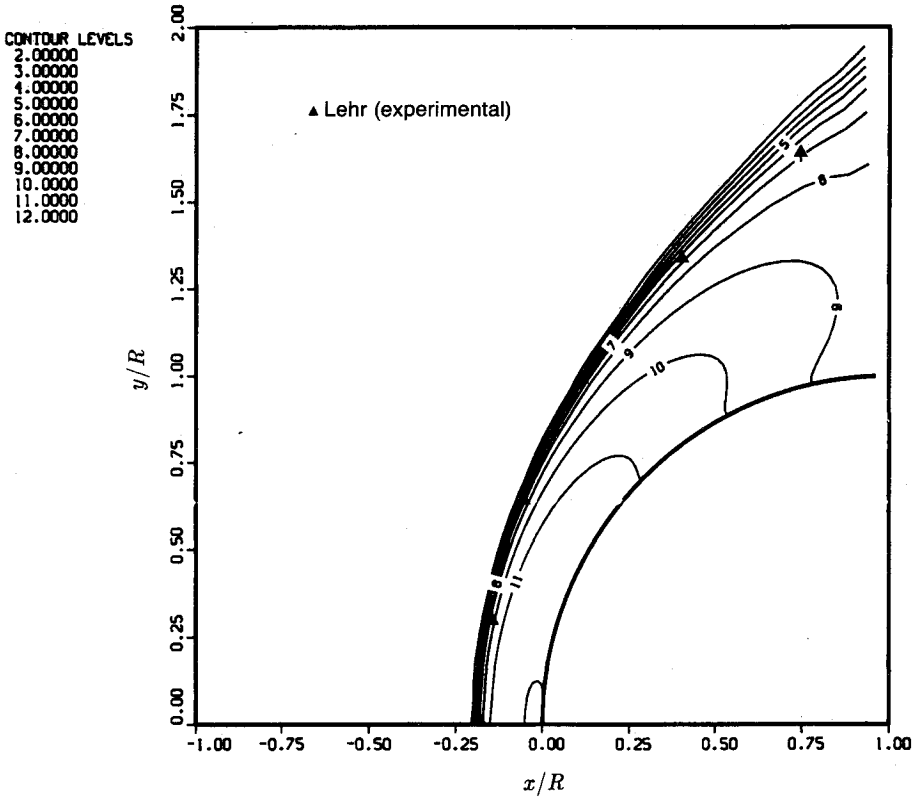

Fig. 10 Temperature contours (T/T_∞) for stoichiometric H_2/air, $M = 6.46$ flow past a sphere. Experimental shock location obtained from Fig. 5 (Ref. 10).

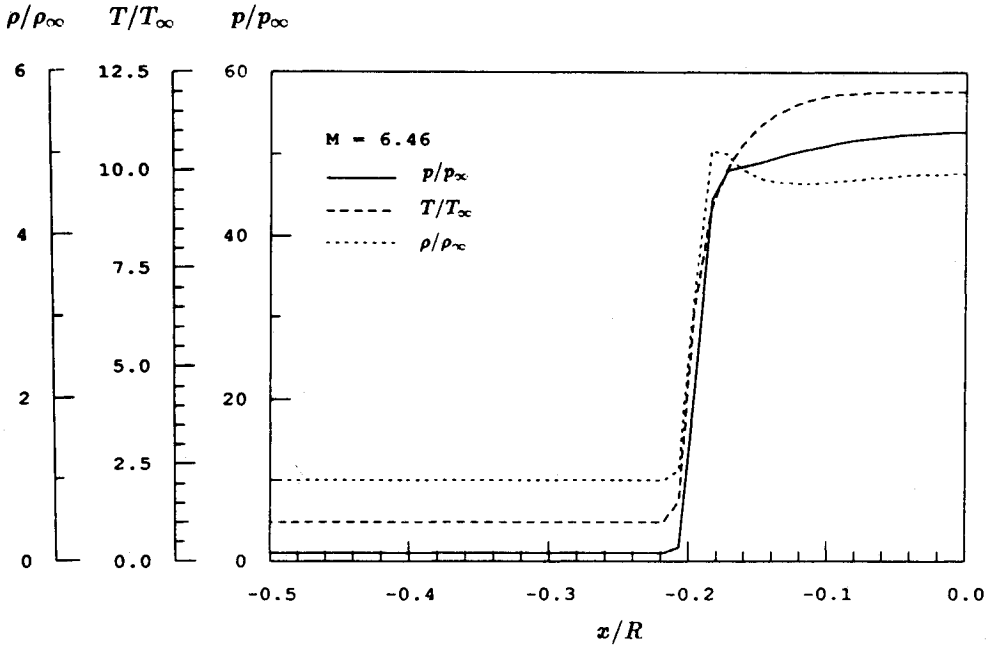

Fig. 11 Distribution of physical quantities along the stagnation streamline for $M = 6.46$ flow past a sphere in a mixture of H_2/air.

tile, which resembles the centerbody of a conventional ramjet, travels through a stationary tube filled with a premixed gaseous fuel and oxidizer mixture. There is no propellant on board the projectile. The tube acts as the outer cowling of the ramjet, and the energy release process travels with the projectile. The pressure, composition, chemical energy density, and speed of sound of the mixture can be controlled to optimize the ballistic efficiency η_b. (Ballistic efficiency is defined here as the ratio of the rate of change of kinetic energy of the projectile to the rate of expenditure of chemical energy.) The concept has the potential for a number of applications, such as hypervelocity impact studies and direct launch to orbit of acceleration insensitive payloads.[28,29]

Several modes of ram accelerator operation have been proposed.[3] In this study, we present results for a shock-induced combustion mode corresponding to that shown in Fig. 1; however, for the projectile configuration considered, a shock-deflagration system rather than a detonation wave was formed.

A projectile configuration having dimensions similar to those of the experimental device currently operating at the University of Washington was chosen. The projectile used in

the present study is composed of two 14-deg half-angle cones and a cylindrical section. The projectile is 19 cm long and has a radius of 1.45 cm. The tube radius is 1.9 cm. A typical propellant fill pressure of 20 atm was selected for our calculations.

Figure 12 shows temperature contours for a mixture of $2H_2+O_2+5He$ and a flight speed $U_1=5.9$ km/s ($M=8.0$). For clarity the plot is magnified in the vertical direction by a factor of 5. Shown in this figure are the nose bow shock and its reflection from the tube wall, followed by a coupled shock-deflagration wave and a series of weaker shock reflections, and, finally, the expansion wave system over the tail of the projectile. Figure 13 shows the temperature distribution along the projectile and tube wall. Note that the ignition temperature is reached behind the second shock reflection, and it is at this point that rapid chemical reactions release energy into the flowing stream, raising its temperature and pressure. The pressure distribution along the projectile and tube wall is shown in Fig. 14. The pressure at the projectile tail is higher than that at the nose, and as a result, a positive thrust force is produced.

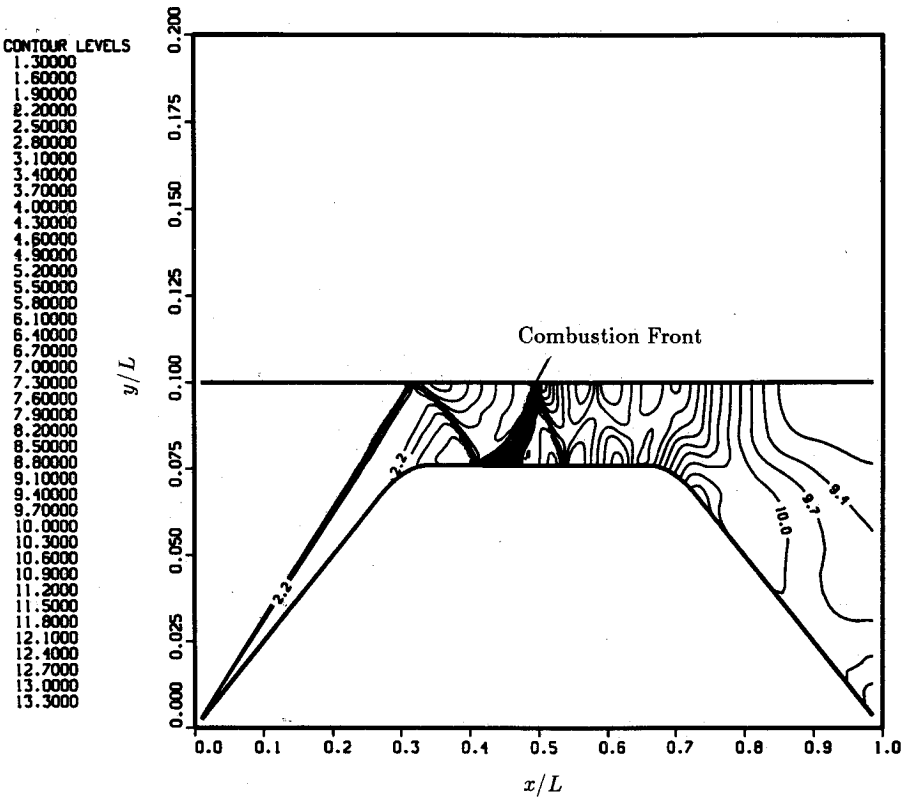

Fig. 12 Temperature contours for a ram accelerator projectile moving at $U_1=5.9$ km/s ($M=8.0$) through a mixture of $2H_2+O_2+5He$.

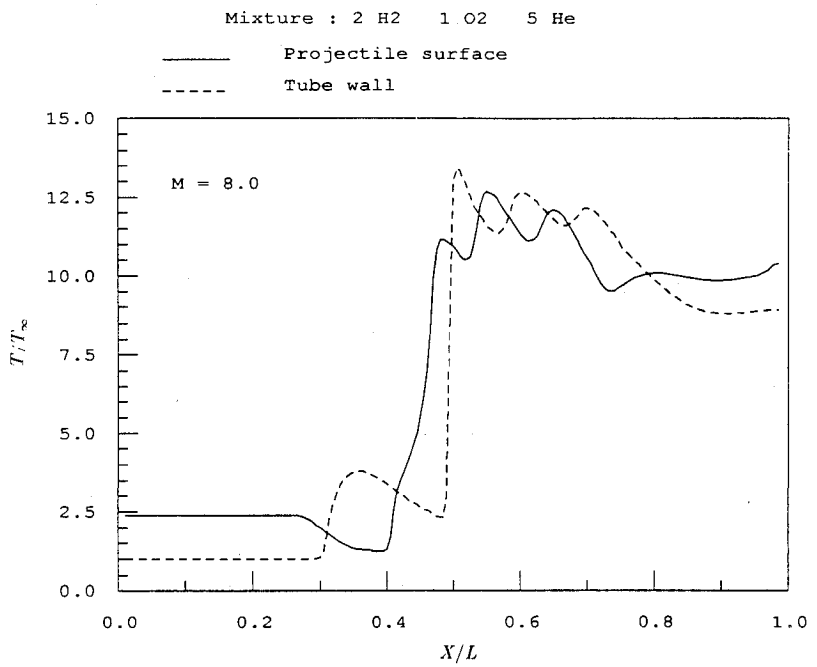

Fig. 13 Temperature distribution along the tube wall and projectile surface for conditions shown in Fig. 12.

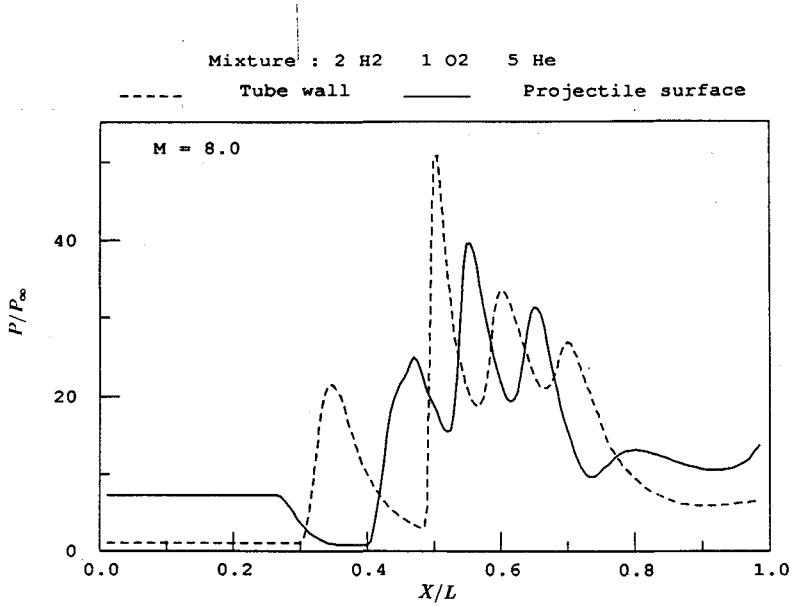

Fig. 14 Pressure distribution along the tube wall and projectile surface for conditions shown in Fig. 12.

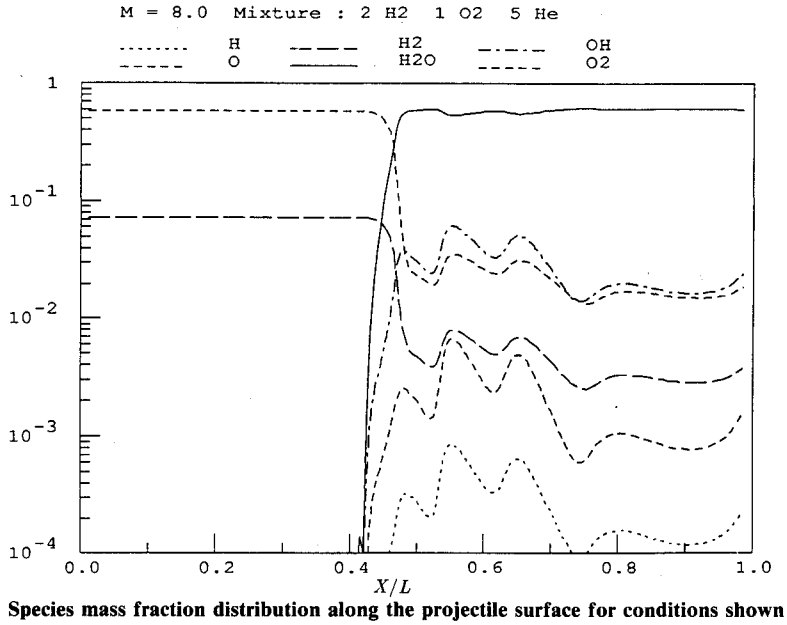

Fig. 15 Species mass fraction distribution along the projectile surface for conditions shown in Fig. 12.

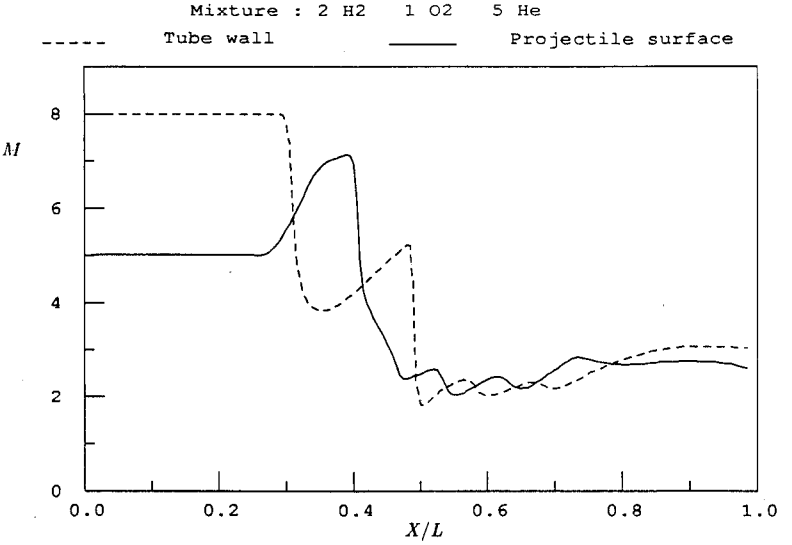

Fig. 16 Mach number distribution along the tube wall and projectile surface for conditions shown in Fig. 12.

The ballistic efficiency η_b can be expressed as

$$\eta_b = \frac{FU_1}{\dot{m}\Delta q} \tag{19}$$

where F is the thrust, $\dot{m}$ is the mass flow rate, and Δq is the heat per unit mass released into the flow. For the case shown in Fig. 12, a ballistic efficiency of 16.3% is obtained.

Figure 15 shows the species mass fraction distribution along the projectile surface. Note that some recombination is taking place at the tail of the projectile, indicating that some of the energy tied up in dissociated material is being converted to useful kinetic energy.

It is important to point out that in this ram accelerator combustion mode, the flow remains supersonic throughout the length of the projectile. This is demonstrated in Fig. 16, which shows the variation of Mach number along the projectile surface and tube wall. The minimum value of the Mach number in this case is $M \approx 2$.

Figures 17–20 show the results obtained for the same configuration but for a higher flight speed $U_1 = 6.7$ km/s ($M = 9.0$).

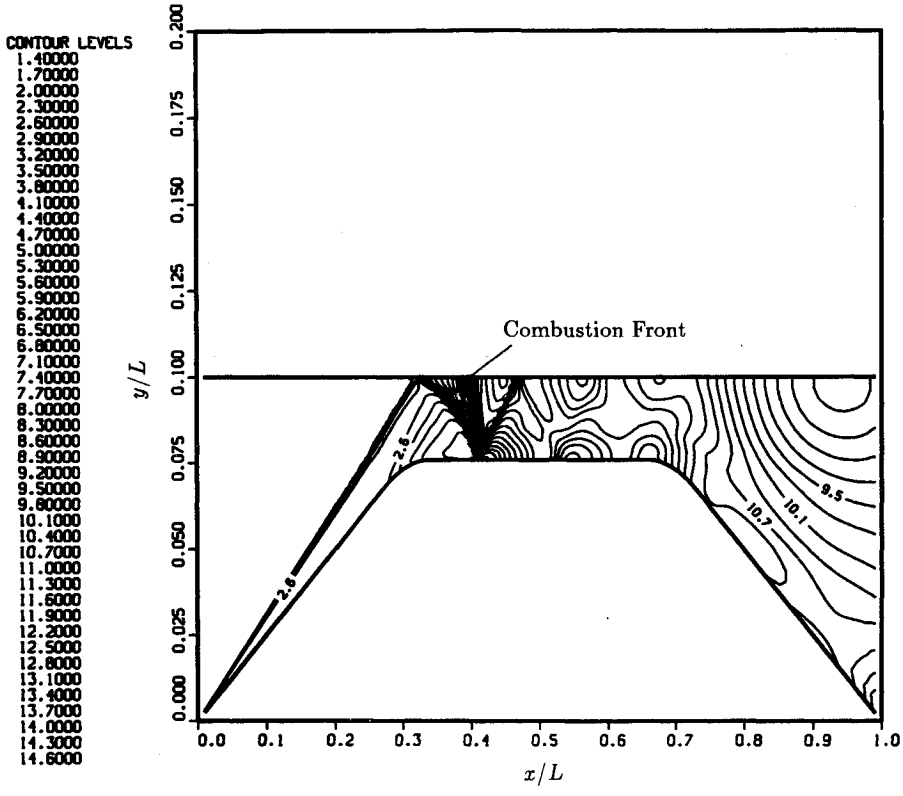

Fig. 17 Temperature contours for a ram accelerator projectile moving at $U_1 = 6.7$ km/s ($M = 9.0$) through a mixture of $2H_2 + O_2 + 5He$.

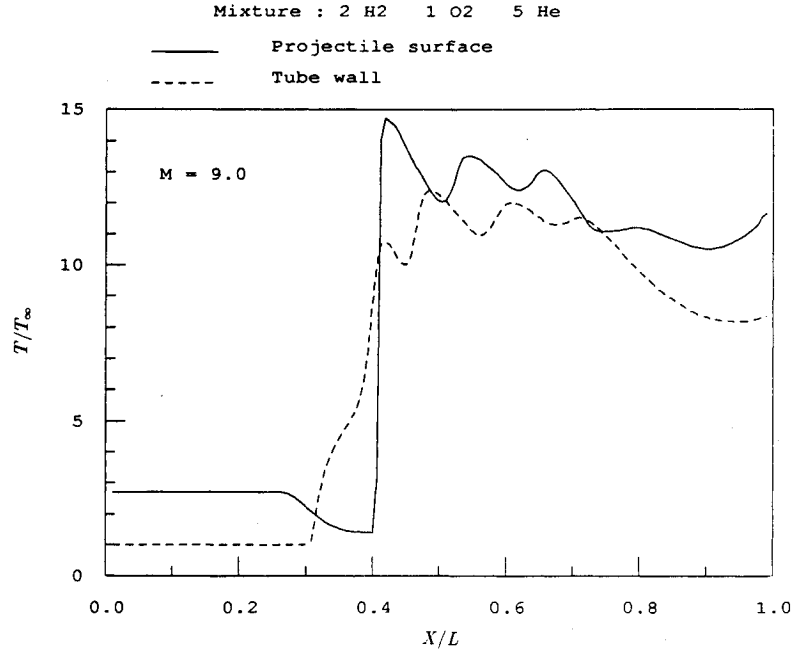

Fig. 18 Temperature distribution along the tube wall and projectile surface for conditions shown in Fig. 17.

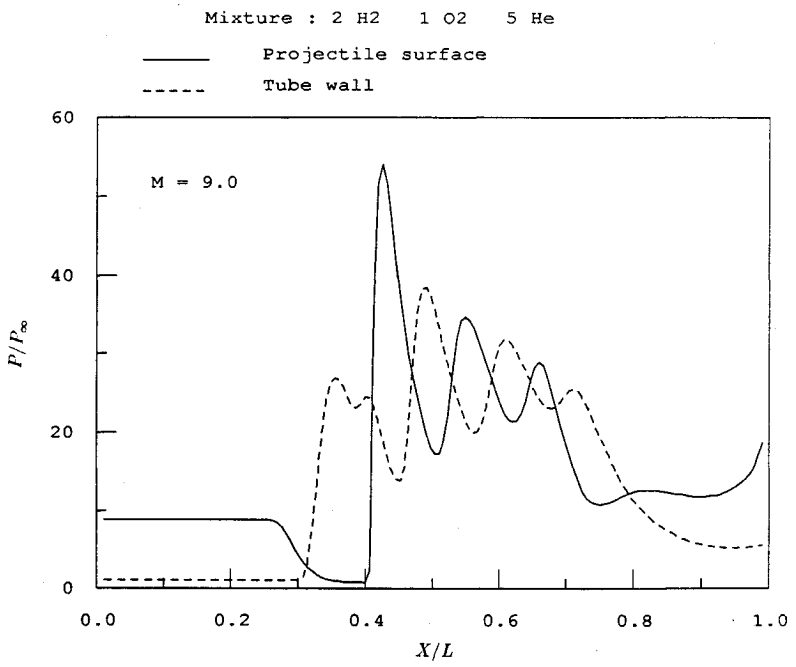

Fig. 19 Pressure distribution along the tube wall and projectile surface for conditions shown in Fig. 17.

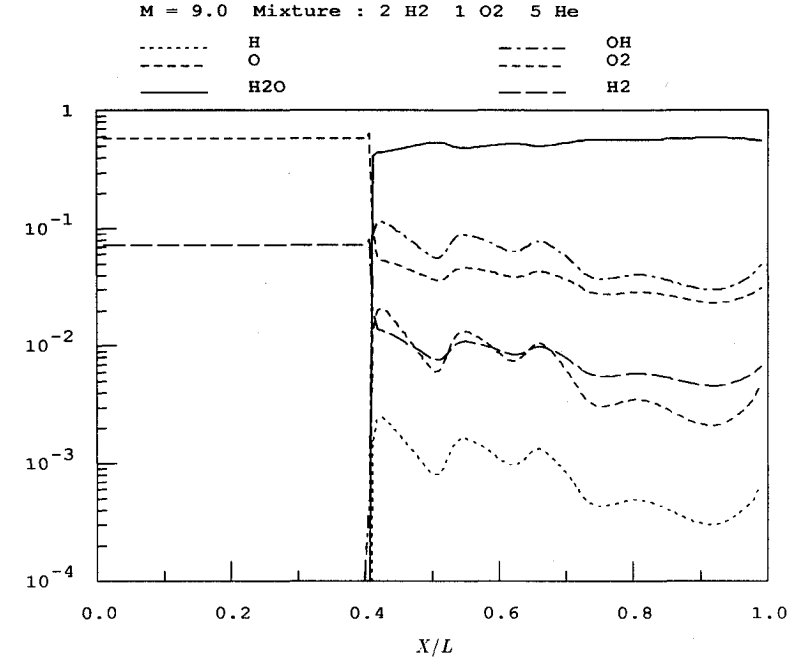

Fig. 20 Species mass fraction distribution along the projectile surface for conditions shown in Fig. 17.

In this case, the ignition temperature is reached behind the first reflected shock, producing a coupled shock-deflagration wave. The ballistic efficiency in this case is 14.5%. Note that due to the effect of the second reflection, which tends to speed up the reactions, the combustion zone at the projectile surface is narrower than at the tube wall. For the present configuration, the energy release of the mixture is not high enough to establish a detonation wave.

The projectile configuration presented here does not represent an optimum shape. Other configurations are currently being studied.[30] Also, experimental investigation of this combustion mode is currently under way at the University of Washington ram accelerator facility.[31]

Conclusions

The various combustion regimes observed in exothermic blunt-body flows, which include coupled and decoupled shock-deflagration systems and combinations of overdriven and oblique detonation waves, were successfully reproduced using a TVD numerical scheme for mixtures of H_2/O_2 and H_2/air. The Euler equations, with the global continuity equation replaced by the species continuity equations, were used in combination with a seven-species/eight-reaction combustion model. The numerical results were compared with previously published experiments. Good agreement between the computed and experimentally observed shock location was obtained. The numerical scheme was also used to investigate a

chemical mass launcher concept known as the ram accelerator in the velocity range of 5–7 km/s. For the configuration studied, the energy release of the mixture was not high enough to establish a detonation wave, and as a result a shock-deflagration system was formed. The combustion front moved forward as the Mach number of the flow increased.

Appendix

The vector $\alpha_{j+\frac{1}{2}}$ appearing in Eq. (16) is given by

$$\alpha_{j+\frac{1}{2}} = \begin{bmatrix} \Delta q_1 - c_1 aa \\ \Delta q_2 - c_2 aa \\ \vdots \\ \Delta q_n - c_n aa \\ (-\xi_y^* u + \xi_x^* v) bb + \xi_y^* \Delta q_{n+1} - \xi_x^* \Delta q_{n+2} \\ \frac{1}{2}\left(aa - \frac{U^*}{a} bb + \frac{\xi_x^*}{a} \Delta q_{n+1} + \frac{\xi_y^*}{a} \Delta q_{n+2} \right) \\ \frac{1}{2}\left(aa + \frac{U^*}{a} bb - \frac{\xi_x^*}{a} \Delta q_{n+1} - \frac{\xi_y^*}{a} \Delta q_{n+2} \right) \end{bmatrix} \tag{A1}$$

with

$$\xi_x^* = \frac{\xi_x}{\sqrt{\xi_x^2 + \xi_y^2}}, \qquad \xi_y^* = \frac{\xi_y}{\sqrt{\xi_x^2 + \xi_y^2}} \tag{A2}$$

$$U^* = \frac{U}{\sqrt{\xi_x^2 + \xi_y^2}} \tag{A3}$$

$$aa = \frac{1}{a^2}\left[\sum_{i=1}^{n} P_{\rho_i} \Delta q_i - p_e (u \Delta q_{n+1} + v \Delta q_{n+2} - \Delta q_{n+3}) \right] \tag{A4}$$

$$bb = \sum_{i=1}^{n} \Delta q_i, \qquad \Delta q = \frac{q_{j+1,k} J_{j+1,k} - q_{j,k} J_{j,k}}{0.5(J_{j+1,k} + J_{j,k})} \tag{A5}$$

It is understood that all of the terms are evaluated at $(j+\frac{1}{2},k)$. The vector $\boldsymbol{R}\Phi$ that appears in Eq. (12) is given by

$$\boldsymbol{R}_{j+\frac{1}{2}}\Phi_{j+\frac{1}{2}} = \begin{bmatrix} \phi^1 + c_1 K_1 \\ \phi^2 + c_2 K_1 \\ \vdots \\ \phi^n + c_n K_1 \\ uK_2 + \xi_y^* \phi^{n+1} + \xi_x^* a K_3 \\ vK_2 - \xi_x^* \phi^{n+1} + \xi_y^* a K_3 \\ HK_2 - \frac{1}{p_e} \sum_{i=1}^{n} a_i^2 \phi^i + aU^* K_3 \\ + (\xi_y^* u - \xi_x^* v)\phi^{n+1} \end{bmatrix} \tag{A6}$$

with

$$K_1 = \phi^{n+2} + \phi^{n+3}, \qquad K_2 = \sum_{\substack{i=1 \\ i \neq n+1}}^{n+3} \phi^i$$

$$K_3 = \phi^{n+2} - \phi^{n+3}$$

where the elements ϕ^l of the dissipation vector are given by Eq. (14). The eigenvalues $a^l_{j+\frac{1}{2}}$ are given by

$$\left(a^1_{j+\frac{1}{2}}, \ldots, a^{n+3}_{j+\frac{1}{2}}\right) = \left(U, \ldots, U, U, U + a\sqrt{\xi_x^2 + \xi_y^2}, U - a\sqrt{\xi_x^2 + \xi_y^2}\right)_{j+\frac{1}{2}} \tag{A7}$$

The frozen sound speed a is

$$a^2 = p_\rho + p_e(H - u^2 - v^2) \tag{A8}$$

with H being the total enthalpy per unit mass. Also the following relations are needed:

$$p_{\rho_i} = \frac{RT}{M_i}(1 - p_e) + p_e\left(\frac{u^2 + v^2}{2} - \int^T c_{p_i}\, dT - h_i^0 \right) \tag{A9}$$

$$p_e = \sum_{i=1}^{n} \frac{c_i}{M_i} \frac{R}{c_v} \tag{A10}$$

$$p_\rho = \sum_{i=1}^{n} c_i p_{\rho_i} \tag{A11}$$

Similar expressions for $\alpha_{k+\frac{1}{2}}$ and $\boldsymbol{R}_{k+\frac{1}{2}}\Phi_{k+\frac{1}{2}}$ are obtained by replacing ξ_x by η_x, ξ_y by η_y, and U by V.

Acknowledgment

This work was supported in part by USAF Contract No. F08635-84-K-0143, ONR Contract No. N00014-88-K-0565, and by a grant from the Olin Corporation. Special thanks go to G. Smeets of the Institut Franco-Allemand de Recherches de Saint-Louis, France, for supplying the authors with the original photographs of the spherical projectiles flying through combustible gas mixtures.

References

[1]Pratt, D. T., Humphrey, J. W., and Glenn, D. E., "Morphology of a Standing Oblique Detonation Wave," AIAA Paper 87-1785, June 1987.

[2]Ostrander, M. J., Hyde, J. C., Young, M. F., Kissinger, R. D., and Pratt, D. T., "Standing Oblique Detonation Wave Engine Performance," AIAA Paper 87-2002, June 1987.

[3]Hertzberg, A., Bruckner, A. P., and Bogdanoff, D. W., "Ram Accelerator: A New Chemical Method for Accelerating Projectiles to Ultrahigh Velocities," *AIAA Journal,* Vol. 26, No. 2, 1988, pp. 195–203.

[4]Bruckner, A. P., Bogdanoff, D. W., Knowlen, C., and Hertzberg, A., "Investigations of Gasdynamic Phenomena Associated with the Ram Accelerator Concept," AIAA Paper 87-1327, June 1987.

[5]Knowlen, C., Bruckner, A. P., Bogdanoff, D. W., and Hertzberg, A., "Performance Capabilities of the Ram Accelerator," AIAA Paper 87-2152, June 1987.

[6]Bruckner, A. P., Knowlen, C., Scott, K. A., and Hertzberg, A., "High Velocity Modes of the Thermally Choked Ram Accelerator," AIAA Paper 88-2925, July 1988.

[7]Ruegg, F. W., and Dorsey, W. W., "A Missile Technique for the Study of Detonation Waves," *Journal of Research of the National Bureau of Standards,* 66C, Jan. 1962, pp. 51–58.

[8]Chernyi, G. G., "Supersonic Flow Around Bodies With Detonation and Deflagration Fronts," *Astronautica Acta,* Vol. 13, 1967, pp. 464–480.

[9]Behrens, H., Struth, W., and Wecken, F., "Shock-Induced Combustion in the Bow Waves of High-Speed Missiles," Deutsch-Französisches Forschungsinstitut, Rept. 2/66, Saint-Louis, France, 1966.

[10]Lehr, H. F., "Experiments on Shock-Induced Combustion," *Astronautica Acta,* Vol. 17, 1972, pp. 589–597.

[11]Bogdanoff, D. W., and Brackett, D. C., "A Computational Fluid Dynamics Code for the Investigation of Ramjet-in-Tube Concepts," AIAA Paper 87-1978, June 1987.

[12]Brackett, D. C., and Bogdanoff, D. W., "Computational Investigation of Oblique Detonation Ramjet-in-Tube Concepts," *Journal of Propulsion and Power,* Vol. 5, No. 3, 1989, pp. 276–281.

[13]Yee, H. C., and Shinn, J. L., "Semi-Implicit and Fully Implicit Shock-Capturing Methods for Nonequilibrium Flows," *AIAA Journal,* Vol. 27, No. 3, 1989, pp. 299–307.

[14]Vincenti, W. G., and Kruger, C. H., *Introduction to Physical Gas Dynamics,* Wiley, New York, 1985, Chap. VII.

[15]Stull, D. R., and Prophet, H., *JANNAF Thermochemical Tables,* 2nd ed., National Bureau of Standards, NSRDS-Rept. 37, June 1971.

[16]Esch, D. D., Siripong, A., and Pike, R. W., "A Technical Report on Thermodynamic Properties in Polynomial Form For Carbon, Hydrogen, Nitrogen and Oxygen Systems From 300 to 15000° K," NASA RFL-TR-70-3, Nov. 1970.

[17]Wada, Y., Kubota, H., Ogawa, S., and Ishiguro, T., "A Diagonalizing Formulation of General Real Gas-Dynamic Matrices With a New Class of TVD Schemes," AIAA Paper 88-3596, July 1988.

[18]Moretti, G., "A New Technique for the Numerical Analysis of Nonequilibrium Flows," *AIAA Journal,* Vol. 3, No. 2, 1965, pp. 223–229.

[19]Evans, J. S., and Schexnayder, C. J., "Influence of Chemical Kinetics and Unmixedness on Burning in Supersonic Hydrogen Flames," *AIAA Journal,* Vol. 18, Feb. 1980, pp. 188–193.

[20]Jachimowski, C. J., "An Analytical Study of the Hydrogen-Air Reaction Mechanism with Application to Scramjet Combustion," NASA TP-2791, Feb. 1988.

[21]Oran, E., Young, T., and Boris, J., "Application of Time-Dependent Numerical Methods to the Description of Reactive Shocks," *Proceedings of the 17th International Symposium on Combustion,* The Combustion Institute, Pittsburgh, PA, 1978, pp. 43–54.

[22]Cambier, J. L., Adelman, H., and Menees, G. P., "Numerical Simulations of an Oblique Detonation Wave Engine," AIAA Paper 88-0063, Jan. 1988.

[23]Bussing, T. R. A., and Murman, E. M., "Finite-Volume Method for the Calculation of Compressible Chemically Reacting Flows," *AIAA Journal,* Vol. 26, No. 9, 1988, pp. 1070–1078.

[24]Candler, G. V., and MacCormack, R. W., "The Computation of Hypersonic Ionized Flows in Chemical Thermal Nonequilibrium," AIAA Paper 88-0511, Jan. 1988.

[25]Eberhardt, S., and Brown, K., "A Shock Capturing Technique for Hypersonic, Chemically Relaxing Flows," AIAA Paper 86-0231, June 1986.

[26]Oran, E. S., and Boris, J. P., *Numerical Simulation of Reactive Flow,* Elsevier, New York, 1987, Chap. 13.

[27]Lee, S., and Deiwert, G. S., "Calculation of Nonequilbrium Hydrogen-Air Reaction with Implicit Flux Vector Splitting Method," AIAA Paper 89-1700, June 1989.

[28]Bruckner, A. P., and Hertzberg, A., "Ram Accelerator Direct Launch System for Space Cargo," 38th Congress of the International Astronautical Federation, Paper IAF-87-211, Oct. 1987.

[29]Kaloupis, P., and Bruckner, A. P., "The Ram Accelerator: A Chemically Driven Mass Launcher," AIAA Paper 88-2968, July 1988.

[30]Yungster, S., and Bruckner, A. P., "A Numerical Study of the Ram Accelerator Concept in the Superdetonative Velocity Range," AIAA Paper 89-2677, July 1989.

[31]Kull, A., Burnham, E., Knowlen, C., Hertzberg, A., and Bruckner, A. P., "Experimental Studies of Superdetonative Ram Accelerator Modes," AIAA Paper 89-2632, July 1989.